Biomolecule-Assisted Hydrothermal Synthesis and Self-Assembly of Bi_2Te_3 Nanostring-Cluster Hierarchical Structure

Jian-Li Mi,[†] Nina Lock,[†] Ting Sun,[‡] Mogens Christensen,[†] Martin Søndergaard,[†] Peter Hald,[†] Huey H. Hng,[‡] Jan Ma,[‡] and Bo B. Iversen[†,*]

[†]Centre for Materials Crystallography, Department of Chemistry and iNANO, Aarhus University, Langelandsgade 140, DK-8000 Aarhus, Denmark, and [‡]School of Materials Science and Engineering, Nanyang Technological University, 50 Nanyang Avenue, Singapore 639798

ABSTRACT A simple biomolecule-assisted hydrothermal approach has been developed for the fabrication of Bi_2Te_3 thermoelectric nanomaterials. The product has a nanostring-cluster hierarchical structure which is composed of ordered and aligned platelet-like crystals. The platelets are ~100 nm in diameter and only ~10 nm thick even though a high reaction temperature of 220 °C and a long reaction time of 24 h were applied to prepare the sample. The growth of the Bi_2Te_3 hierarchical structure appears to be a self-assembly process. Initially, Te nanorods are formed using alginic acid as both reductant and template. Subsequently, Bi_2Te_3 grows in a certain direction on the surface of the Te rods, resulting in the nanostring structure. The nanostrings further recombine side-by-side with each other to achieve the ordered nanostring clusters. The particle size and morphology can be controlled by adjusting the concentration of NaOH, which plays a crucial role on the formation mechanism of Bi_2Te_3. An even smaller polycrystalline Bi_2Te_3 superstructure composed of polycrystalline nanorods with some nanoplatelets attached to the nanorods is achieved at lower NaOH concentration. The room temperature thermoelectric properties have been evaluated with an average Seebeck coefficient of $-172\ \mu V\ K^{-1}$, an electrical resistivity of $1.97 \times 10^{-3}\ \Omega m$, and a thermal conductivity of $0.29\ W\ m^{-1}\ K^{-1}$.

KEYWORDS: self-assembly · hierarchical nanostructure · thermoelectric materials · bismuth telluride · hydrothermal synthesis

Thermoelectric semiconductors have attracted much attention for their applications in power generation and solid-state refrigeration with many features such as long life, no moving fluids or moving parts, no emissions of toxic gases, low maintenance, silent function, and high reliability.[1,2] Due to the demands of more efficient materials for alternative energy production and utilization, an increasing emphasis can be expected on the development of advanced thermoelectric materials which may play a key role in the future. Bismuth telluride (Bi_2Te_3)-based alloys are the most commonly used thermoelectric materials at ambient temperature. There have been persistent efforts to improve the thermoelectric performance of Bi_2Te_3 and its alloys.[3−5]

Nanostructuring of thermoelectric materials is an effective approach to improve the thermoelectric figure of merit (ZT), which for commercial bulk materials typically is around unity. The size dependence of the physical properties becomes evident when the size of the building blocks of the material is reduced to nanometer scale. Theoretical predictions and experimental investigations have suggested that nanostructuring of thermoelectric materials can result in enhancements in ZT, owing to both a high density of states and an increased phonon scattering causing reduced lattice thermal conductivity.[4−12] Quantum dot superlattice structures, which have discrete energy levels due to the quantum confinement, potentially result in a more favorable carrier scattering mechanism and a much lower lattice thermal conductivity. The thermoelectric performance can be enhanced by controlling the transport of phonons and electrons in the superlattice materials. A maximum ZT value of about 2.4 was observed for a p-type Bi_2Te_3/Sb_2Te_3 superlattice thin film,[4] and a ZT value of 3 was also reported for an n-type PbSeTe/PbTe quantum dot superlattice.[13] Despite the high ZT values reported in superlattice structures, it is difficult to use them in large-scale energy conversion applications. It has been suggested that the primary cause of ZT enhancement in superlattices can also exist in random nanostructures,[5,9] and hence, nanostructured thermoelectric materials can have an advantage when assembled into desired shapes for device applications. Recently, it was reported that a high ZT value of 1.4 at 100 °C was achieved

*Address correspondence to bo@chem.au.dk.

Received for review September 28, 2009 and accepted April 13, 2010.

Published online April 20, 2010.
10.1021/nn100267q

in a p-type nanocrystalline $Bi_xSb_{2-x}Te_3$ bulk alloy prepared by hot pressing of nanopowders that were produced by ball-milling of crystalline $Bi_xSb_{2-x}Te_3$ ingots.[5] The enhanced ZT value is mainly the result of a significant reduction in thermal conductivity due to the strong phonon scattering by grain boundaries and defects in the nanostructures.

Various chemical synthesis methods have been reported for preparation of Bi_2Te_3-based alloys, including chemical alloying,[14] reverse micelle chemistry,[15] microwave-assisted wet chemical methods,[16] electrodeposition,[17,18] as well as other procedures.[19−21] Different morphologies of Bi_2Te_3, such as nanorods,[22] nanotubes,[6,20] hexagonal platelets,[16,21,23,24] and nanowires,[25] have been reported using various chemical routes. Among them, one of the convenient and highly efficient methods for preparation of nanostructured Bi_2Te_3-based materials is the surfactant-mediated solvothermal/hydrothermal technique. Most work on solvothermal or hydrothermal synthesis of Bi_2Te_3 involves reduction of Bi and Te precursor compounds (or of tellurium powder directly) by $NaBH_4$,[6,26] N_2H_4,[27] or organic solvents such as dimethylformamide (DMF)[28] or ethylene glycol[23] in the presence of surfactants such as cetyltrimethylammonium bromide (CTAB) or ethylenediaminetetraacetic acid (EDTA). However, the products usually consist of large particles with broad size distributions and multiple morphologies. The reason is probably that the reductive powers of the reducing agents are too strong, making it difficult to control the process.

There has been an increased emphasis on the topic of "green" chemistry and chemical processes.[29,30] Most of the chemical routes for the preparation of Bi_2Te_3-based compounds reported to date rely on toxic reducing agents such as hydrazine, $NaBH_4$, or DMF and organic solvents. Environmentally benign reducing agents and the nontoxic solvent media are some of the key issues that merit important consideration in a green synthetic strategy.[30] As an example of a green chemistry reducing approach, glucose has been reported as the reducing agent in the synthesis of silver nanoparticles.[30] It has also been reported that the biomolecule alginic acid, which is a straight-chain polyuronic acid, can be used as a mild reducing agent for synthesis of single-crystalline tellurium nanowires.[31] Besides the reductive properties of the biomolecules, they also have strong size or shape directing functionality in the reaction process, which can possibly be exploited to organize nanostructured materials with special morphologies.

In this work, we introduce a green and high yield (about 90%) hydrothermal method to prepare Bi_2Te_3 compounds with nanostring-cluster hierarchical structures using alginic acid as the reducing agent. The hierarchical structure consists of well-oriented nanoplatelets with an edge length of ~100 nm and a thickness of ~10 nm. The sizes can be controlled by adjusting the concentration of NaOH. The formation mechanism, the effect of NaOH concentration, as well as the thermoelectric properties of the hierarchical nanostructured Bi_2Te_3 are reported.

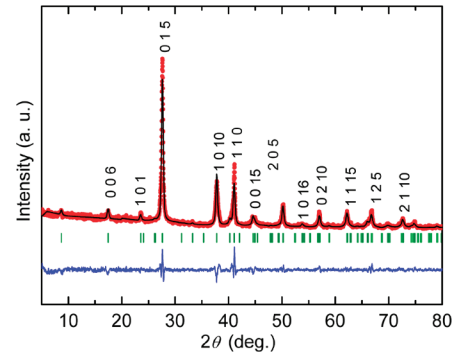

Figure 1. Observed and calculated diffraction patterns and the difference profile for the Bi_2Te_3 powder prepared at 220 °C for 24 h in 0.2 M NaOH. Space group *R*-3*m*, a = 4.398(1) Å, c = 30.48(1) Å, z(Bi) = 0.4008(3), z(Te_2) = 0.7924(2), R_I = 6.84%, R_F = 5.69%.

RESULTS AND DISCUSSION

The phase purity and the crystallographic structure of the products were determined by X-ray diffraction (XRD). Structural Rietveld refinements were performed on XRD data recorded on the Bi_2Te_3 powder prepared at 220 °C for 24 h in 0.2 M NaOH. Figure 1 shows the observed and calculated diffraction patterns and the difference profile. All of the detected peaks can be well indexed to the rhombohedral Bi_2Te_3 crystal structure (JCPDS No. 82-0358), indicating that Bi_2Te_3 has been successfully synthesized by the biomolecule-assisted hydrothermal route. The observed relative intensities of the (1 0 10) and (1 1 0) peaks are abnormal relative to those of the calculated pattern (and also the JCPDS card), indicating anisotropic growth of Bi_2Te_3 during the synthesis, which leads to preferred orientation effects in the PXRD data measured on a flat sample holder. The lattice parameters from the Rietveld refinement are a = 4.398(1) Å and c = 30.48(1) Å, in good agreement with the standard data of a = 4.395 Å and c = 30.44 Å.[32] The particle sizes were determined by the Scherrer equation through fitting the peaks by a Lorentz function. A silicon standard was used to account for the instrumental broadening. The particle sizes calculated along the [0 1 5] and [1 0 10] directions are around 46 and 28 nm, respectively, confirming the anisotropic growth of the sample prepared at 220 °C for 24 h in 0.2 M NaOH. From the geometrical relationship between the [0 1 5] direction and the *ab* plane, the particle size along the *ab* plane is evaluated to be about 37 nm. Similarly, from the geometrical relationship between the [1 0 10] direction and the *c*-axis, the particle size of the *c*-direction is calculated to be about 23 nm. The results show that the particles of the product are nanosized and have platelet-like structures.

The morphologies and sizes of the products were investigated by field-emission scanning electron microscopy (FESEM) and transmission electron microscopy (TEM). Figure 2a,b shows typical SEM images in different magnifications of the Bi_2Te_3 powders prepared at 220 °C for 24 h in 0.2 M NaOH. The SEM images show a large number of hierarchical structures, each of which consists of arrays of very small nanoplatelets. Details of the hierarchical structures can be seen in the TEM images as shown in Figure 2c,d. The hierarchical structures consist of nanoplatelets which order and align into strings. These strings connect side-by-side to form the string clusters. Figure 2c shows a two-string cluster, and Figure 2d shows a multi-string cluster structure. The TEM images and the selected area electron diffraction (SAED) pattern (see the inset of Figure 2d) suggest that the nanoplatelets in the nanostring clusters possess an orientational crystallographic relationship. If there had been a random orientation between individual particles, electron diffraction rings would have been observed rather than diffraction spots. Diffuse scattering is observed pointing to a slight mismatch in crystallographic orientation of the stacked nanocrystals. The nanoplatelets are uniform in particle size with diameters of ~100 nm (or even smaller) and thicknesses of ~10 nm, which are much smaller than previously reported Bi_2Te_3[16] or Sb_2Te_3[24] nanoplatelets, despite the high reaction temperature of 220 °C and the long reaction time of 24 h that were used in the present study. The results are consistent with the XRD results.

The crystallographic relationship of the nanoplatelets and the local chemical composition were analyzed by high-resolution TEM (HRTEM) and energy-dispersive X-ray analysis (EDX). Figure 3a is a TEM image of the hierarchical structure. The HRTEM image in Figure 3b was taken from the edge area of this structure. The HRTEM clearly shows that the well-resolved 2D diffraction fringes among the different platelets are uniform with a plane spacing of 1.01 nm, which corresponds to the (0 0 3) lattice planes in rhombohedral Bi_2Te_3. The result indicates the nanoplatelets almost have the same orientational relationship along the *c*-axis direction, which may be explained by the anisotropic crystallographic structure of Bi_2Te_3. The Bi_2Te_3 crystal consists of a layered structure along the *c*-axis (parallel to the [0 0 3] direction) with weak van der Waals bonds between the neighboring Te layers. The crystal growth rate perpendicular to the *c*-axis is much higher than that parallel to the *c*-axis direction because the crystalline facets tend to develop on the low-index planes to minimize the surface energy. The dots shown in Figure 3c,d represent the chemical composition distributions of Te and Bi, respectively, in the structure shown in Figure 3a. Bi and Te are distributed homogeneously in the hierarchical structure, indicating the structure is a Bi−Te compound.

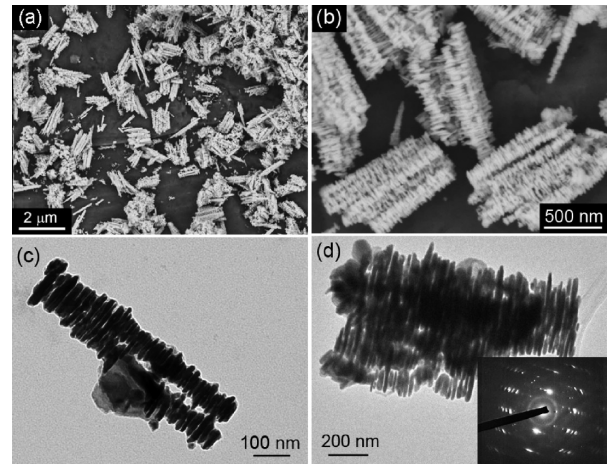

Figure 2. (a,b) SEM images of the Bi_2Te_3 hierarchical structures. (c) TEM image of a two-string cluster. (d) TEM image of a multi-string cluster hierarchical structure with the corresponding SAED pattern as the inset.

Figure 4a is a TEM image showing another superstructure which is also occasionally observed in the sample prepared at 220 °C for 24 h in 0.2 M NaOH. Besides the ordered nanoplatelets, some smooth nanorods are detected in the structure. It can be demonstrated that the nanoplatelets with well-controlled orientation are attached on the nanorods, which suggests the nanoplatelets nucleate on and grow out of the rods. Detailed EDX mapping analysis was performed on the structure to study the local chemical composition. The dots shown in Figure 4b,c represent Te and Bi, respectively. The mapping analysis gives direct evidence of the chemical compositions for the rods and platelets. Both elements Bi and Te are detected in the area of the nanoplatelets, but only Te is detected in the area of the rods. Therefore, it can be concluded that the nanoplatelets are composed of Bi_2Te_3, while the smooth nanorods are composed of elemental Te.

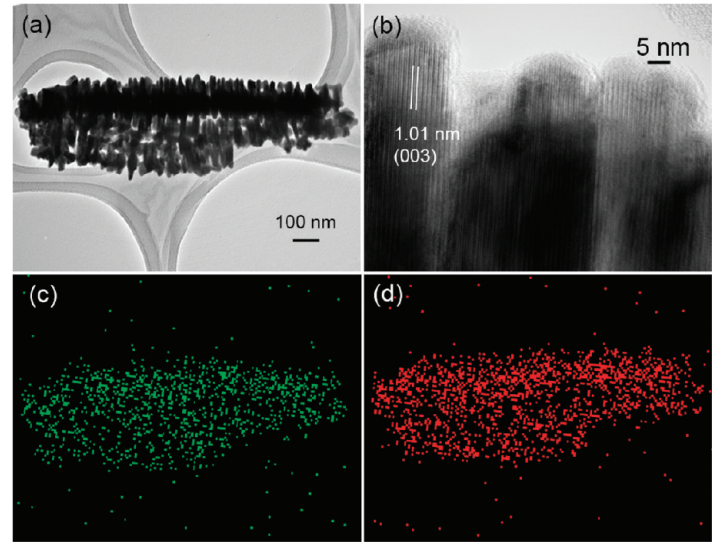

Figure 3. (a) TEM image of a hierarchical structure. (b) HRTEM image taken from the edge area of the hierarchical structure. (c,d) EDX mapping analysis of the element distributions of Te (c) and Bi (d) in the structure.

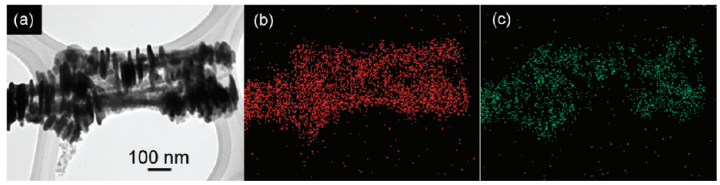

Figure 4. (a) TEM image of the structure with nanoplatelets attached on the nanorods. (b,c) EDX mapping of the element distributions of Te (b) and Bi (c) in the structure.

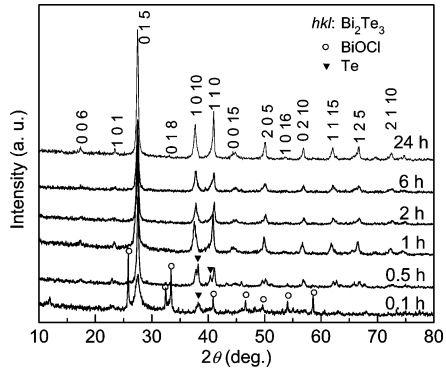

Figure 5. XRD patterns of the samples prepared at 220 °C in 0.2 M NaOH at different reaction times of 0.1, 0.5, 1, 2, 6, and 24 h.

Consequently, elemental Te is suggested to be an intermediate product during the synthesis process. The structure is similar to that reported by Lu *et al.* using a high-temperature organic solution approach, and an epitaxial orientation relationship between the platelets and the matrix (Te rod) was suggested.[21] This intermediate Te rod/Bi_2Te_3 platelet composite morphology proposes a possible formation mechanism of Bi_2Te_3 hierarchical structure, which will be discussed later.

Figure 5 shows the XRD patterns of the samples prepared at 220 °C at different reaction times with a NaOH concentration of 0.2 M. According to the XRD results, the hydrolyzed product BiOCl and elemental Te were the main phases detected in the sample with a reaction time of 0.1 h. In contrast, both Te and Bi_2Te_3 were found in the sample with a reaction time of 0.5 h. The excessive Bi possibly exists as ions in the solution. Almost phase-pure Bi_2Te_3 was detected after a reaction time of 1 h. No metallic Bi was detected in the process; therefore, a possible mechanism explaining the reaction between TeO_3^{2-} ions and metal Bi^{3+} ions can be suggested. TeO_3^{2-} ions are first rapidly reduced into elemental Te by alginic acid under the hydrothermal condition in NaOH aqueous solution. Subsequently, Te acts as an intermediate product in the process to form Bi_2Te_3. The formation of Bi_2Te_3 appears to result from direct reaction of metallic Te with either simple Bi^{3+} ions or complex $[Bi(EDTA)]^+$ ions. The process is consistent with the EDX mapping analysis of the Te rod/Bi_2Te_3 platelet structure shown in Figure 4, where the Bi_2Te_3 nanoplatelets are grown from the Te nanorods. A similar reaction process of Bi_2Te_3 was previously reported.[25] The results also provide the direct evidence for the self-assembly of the Bi_2Te_3 hierarchical superstructure where intermediate Te is used as templates as described below.

On the basis of the above analysis, a self-assembly growth mechanism can be proposed for the formation of the Bi_2Te_3 hierarchical structures. Initially, Te nanorods are formed from TeO_3^{2-} in a fast reaction using alginic acid as reducing agent under the mild hydrothermal conditions (Figure 6a). In this step, alginic acid might also serve as a template for the synthesis of the Te nanorods. It has been proposed that a large number of hydroxyl groups on the surface of alginic acid could react with Te precursor to form chain-shaped intermediates which could decompose to form elemental Te upon reduction. Thereby, the linear structure of the intermediates directs the growth of the Te nanorods.[31] In the next step, Bi_2Te_3 nanoplatelets grow in a certain direction using the Te rods as templates, as suggested in Figure 6b. Because of the anisotropic crystallographic structure, the Bi_2Te_3 crystals tend to develop platelet-like structure. Then, the Bi_2Te_3 nanostrings are formed with the growth of Bi_2Te_3 nanoplatelets, while the Te rods are diminished. Simultaneously, the strings connect to each other side-by-side due to the combination of nanoplatelets with certain orientation (Figure 6c,d). Finally, the single phase of Bi_2Te_3 consisting of nanostring-cluster hierarchical structures is formed with well-ordered arrays (Figure 6e). The above self-assembly of the hierarchical structure can even be verified by the different morphologies of the intermediate products (shown in Figure 7).

Even smaller nanostructures of Bi_2Te_3 can be obtained when the concentration of NaOH is decreased. Figure 8a,b shows the SEM and TEM images of the sample prepared in 0.1 M NaOH at 220 °C for 24 h.

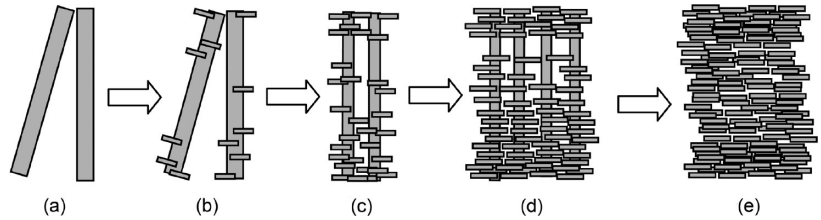

Figure 6. Suggested self-assembly mechanism of the Bi_2Te_3 hierarchical nanostructure. (a) Te nanorods. (b,c,d) Te rod/Bi_2Te_3 platelet composites. (e) Bi_2Te_3 hierarchical structure.

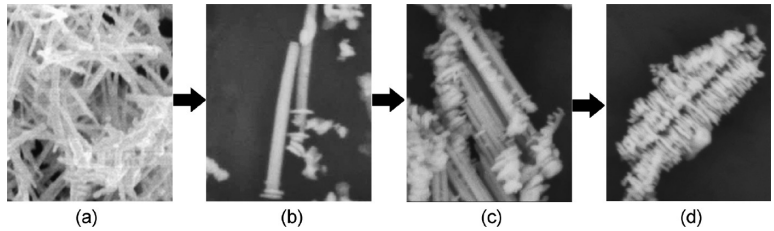

Figure 7. SEM images of various morphologies suggesting the self-assembly process for the Bi_2Te_3 hierarchical structure. (a) Te nanorods. (b,c) Te rod/Bi_2Te_3 platelet composites. (d) Bi_2Te_3 hierarchical structure.

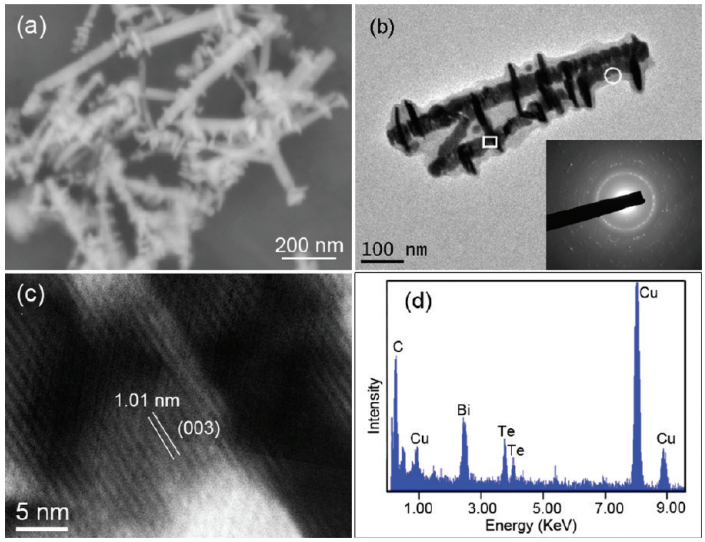

Figure 8. (a) SEM image of Bi_2Te_3 nanorods with some nanoplatelets attached on the rods prepared at 220 °C for 24 h in 0.1 M NaOH. (b) TEM image and SAED pattern. (c) HRTEM image taken from the selected rectangular area in (b). (d) EDX spectra acquired from the selected circular area of the nanorod matrix shown in (b).

Both the SEM and the TEM images show that the products are composed of small nanorods with some nanoplatelets attached to the nanorods. However, unlike the structure shown in Figure 4a or Figure 7b,c, local chemical composition analysis indicates that the nanorod of this structure matrix is Bi_2Te_3 rather than elemental Te, which agrees with the XRD result showing a very pure phase in the product. TEM images and SAED analysis show that the nanorod matrix is a polycrystalline structure. The polycrystalline Bi_2Te_3 nanorods, composed of small nanoparticles, have lengths up to 500 nm and diameters ranging from about 20 to 50 nm. The particle sizes calculated from XRD are about 35 and 22 nm along (0 1 5) and (1 0 10), respectively. The results show that the nanostructure prepared in 0.1 M NaOH is much smaller than that prepared in 0.2 M NaOH. It is found that the Te rods first formed in lower NaOH concentration are much smaller than those in higher NaOH concentration, which probably affects the resulting structure size of Bi_2Te_3. The well-resolved diffraction fringes shown in the HRTEM image in Figure 8c indicate that the nanocrystalline rods and the nanoplatelets almost have the same orientation relationships with the direction of [0 0 3] parallel to the rods. Figure 8d is the EDX result recorded from the polycrystalline nanorod matrix. Both Bi and Te are detected on the nanorods. The signals for Cu and C peaks originate from the sample holder.

Figure 9 shows the XRD patterns of the samples prepared at 220 °C for 24 h with different concentrations of NaOH. As described above, almost single-phase Bi_2Te_3 can be obtained using 0.1 or 0.2 M NaOH. However, when the NaOH concentration is increased to 0.4 M, pure phase of Bi_2Te_3 cannot be achieved even after a reaction time of 24 h at 220 °C. Impurities of metallic Bi and Te coexist in this sample. A SEM image (Figure 10a) shows that the sample consists of large nanorods and small particles. When the concentration of NaOH is further increased to 0.8 and 1.6 M, the XRD patterns show that well-crystallized Bi_2Te_3 is obtained. Larger particles with similar morphologies are obtained for the two samples prepared in 0.8 and 1.6 M NaOH. Figure 10b is a typical SEM image of the sample prepared in 1.6 M NaOH. The sizes of the particles are approximately 100−300 nm. The difference in particle size between the 0.1/0.2 M samples in comparison with the 0.8/1.6 M samples agrees well with the XRD results. The broad XRD peaks observed for the samples prepared in 0.1 and 0.2 M NaOH indicate that they are composed of small particles, while the sharp peaks of samples prepared in 0.8 and 1.6 M NaOH indicate large

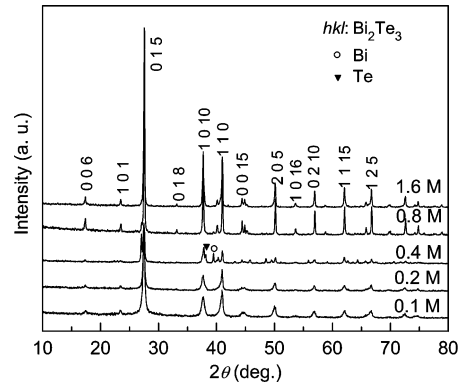

Figure 9. XRD patterns of the samples prepared at 220 °C for 24 h with different NaOH concentrations of 0.1, 0.2, 0.4, 0.8, and 1.6 M.

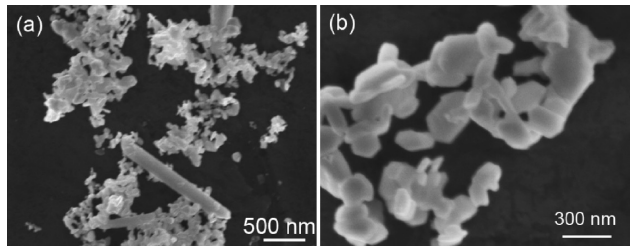

Figure 10. SEM images of the samples prepared at 220 °C for 24 h in (a) 0.4 M and (b) 1.6 M NaOH.

particles. The NaOH concentration possibly affects the reduction of Bi^{3+}, which influences the formation of Bi_2Te_3. A separate experiment shows that Bi cannot be reduced from Bi^{3+} in the absence of NaOH. Hence, it is likely that the reduction of Bi is weak in NaOH concentrations of 0.1 and 0.2 M, such that the formation process of Bi_2Te_3 results from a reaction of metallic Te with Bi^{3+} (or $[Bi(EDTA)]^+$) ions. The rate of the reduction of Bi is much faster in higher NaOH concentration. Both metallic Bi and Te were detected as intermediate phases in the synthesis using 0.8 and 1.6 M NaOH. Therefore, in this case, the main reaction mechanism is not the same as that at low NaOH concentration. The Bi_2Te_3 formation mechanism at high NaOH concentration is suggested to be as follows. First, TeO_3^{2-} ions and Bi^{3+} ions are reduced to elemental Te and Bi, respectively. Second, the two elements react with each other to form telluride products, a mechanism which is similar to the formation of CoTe nanowires.[33] The two Bi_2Te_3 formation mechanisms probably coexist at the intermediate NaOH concentration of 0.4 M. However, the reactivity for the combination between elemental Bi and Te might be weaker in this case than at high NaOH concentration (0.8/1.6 M), and thus the metallic phases of Bi and Te coexist with Bi_2Te_3 in the product prepared in 0.4 M NaOH. Moreover, the NaOH concentration additionally affects the morphology and size of the intermediate products, the Te nanorods, which affect the final morphology and the crystallite size of the Bi_2Te_3. It is found that the Te nanorods formed in 0.4 M NaOH are much larger than those formed in lower NaOH concentration, and it becomes more difficult to consume all of the Te rods. As a result, some smooth Te nanorods remain in the product prepared in 0.4 M NaOH. The concentration of NaOH, which affects the reduction rate of Bi, the size of Te nanorods, as well as the formation mechanism of Bi_2Te_3, is important to form the hierarchical structure.

Because the intrinsic thermoelectric properties of the hierarchical nanostructures are difficult to evaluate, the Bi_2Te_3 powders prepared at 220 °C for 24 h in 0.2 M NaOH have been sintered into bulk pellets by spark plasma sintering (SPS) to measure the thermoelectric properties. The thermopower of the pellet was analyzed by a potential Seebeck microprobe (PSM) at room temperature. Figure 11 shows the distribution of the Seebeck coefficient in the selected area. An average Seebeck coefficient of $-172.22\ \mu V\ K^{-1}$ is achieved. The Seebeck coefficient has a broad distribution ranging from about -120 up to $-250\ \mu V\ K^{-1}$, which might be due to local composition inhomogeneities in the sample. The room temperature electrical resistivity and thermal conductivity were also evaluated. An electrical resistivity of $1.97 \times 10^{-3}\ \Omega m$ and a thermal conductivity of $0.29\ W\ m^{-1}\ K^{-1}$ have been achieved. The nanostructure is expected to decrease the thermal conductivity. Besides the very low density of the bulk sample with a relative density of ~55%, the nanostructure should also result in low thermal conductivity. The nanoplatelets obtained in the conditions of 0.1 and 0.2 M NaOH are much smaller than most of the previously reported Bi_2Te_3 particles prepared by hydrothermal methods, and the particle size can further be controlled by adjusting the concentration of NaOH. However, the ZT value of the bulk sample

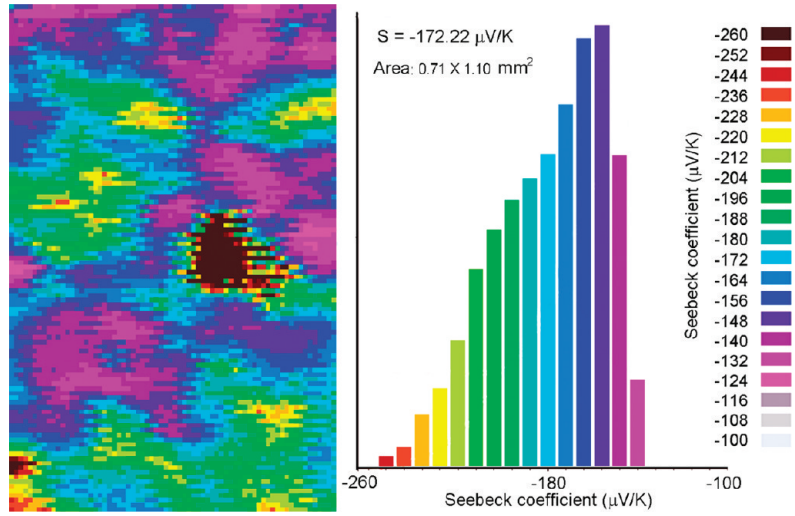

Figure 11. Thermopower resolution of the selected 0.71 × 1.10 mm² area at room temperature. An average Seebeck coefficient of $-172.22\ \mu V\ K^{-1}$ is achieved.

is limited by the relative high electrical resistivity, which probably is due to the low quality of the bulk sample with only about ~55% relative density. As a result, a ZT value of 0.016 is obtained. The thermoelectric properties should possibly be optimized by adjusting the carrier concentration and achieving high-quality bulk samples.

CONCLUSIONS

In summary, a green, facile, and high-yield biomolecule-assisted hydrothermal approach has been developed for the fabrication of Bi_2Te_3 thermoelectric materials. Nanostring-cluster hierarchical structure of Bi_2Te_3 was prepared at a reaction temperature of 220 °C for 24 h in 0.2 M NaOH. The structure consists of ordered and aligned platelet-like nanocrystals. The possible self-assembly growth mechanism of the hierarchical structure was suggested based on PXRD and electron microscopy experimental results. Te nanorods are formed initially using alginic acid as reductant. Bi_2Te_3 nanoplatelets grow from Te rods to form the string-like structure, and the nanostrings are combined side-by-side, resulting in the hierarchical structure. NaOH plays a crucial role in the formation mechanism on phase purity, structure, and morphology. A room temperature Seebeck coefficient of $-172.22\ \mu V\ K^{-1}$, an electrical resistivity of $1.97 \times 10^{-3}\ \Omega m$, and a thermal conductivity of $0.29\ W\ m^{-1}\ K^{-1}$ are obtained for the SPS sintered bulk sample. The thermoelectric properties could be further optimized by adjusting the carrier concentration and achieving high-quality bulk samples.

METHODS

All of the chemical reagents used in the experiment were analytical grade. In a typical procedure for the synthesis of hierarchical nanostructured Bi_2Te_3, 0.5 mmol EDTA was dissolved in 12 mL of distilled water in a Teflon-lined, stainless steel autoclave with a capacity of 15 mL; 0.25 mmol $BiCl_3$ and 0.375 mmol K_2TeO_3 were mixed with 0.4 g of alginic acid in the above solution. Finally, NaOH was added to get the target NaOH concentration of about 0.2 M. After stirring the solution for several minutes, the autoclave was sealed and maintained at 220 °C for 24 h and then allowed to cool in air to room temperature. The black products were collected and washed with distilled water and ethanol by centrifugation. The product yield is about 90%. Experiments with different reaction times from 0.1 to 24 h and different NaOH concentrations from 0.1 to 1.6 M were also performed to further study the formation mechanism of the hierarchical structure.

The X-ray diffraction (XRD) patterns were measured on a STOE powder diffractometer using Cu Kα radiation ($\lambda = 1.5406$ Å). The morphology of the products was observed on a NOVA600 field-emission scanning electron microscope (FESEM). Transmission electron microscopy (TEM), high-resolution TEM (HRTEM), and selected area electron diffraction (SAED) of the structures were performed on a Philips CM20 microscope and a JEM-2010F microscope. The local chemical compositions of the structure were also analyzed on the JEM-2010F microscope with an energy-dispersive X-ray (EDX) spectrometer. The Bi_2Te_3 powder prepared at 220 °C for 24 h in 0.2 M NaOH was sintered into bulk by spark plasma sintering (SPS) at 350 °C under 40 MPa for 5 min. The thermoelectric power was measured by a potential Seebeck microprobe (PSM)[34] at room temperature. The electrical resistivity was measured by a four-probe method, and the thermal conductivity was measured with a laser flash apparatus (Netzsch LFA 457).

Acknowledgment. The work was supported by the Danish Strategic Research Council (Centre for Energy Materials), the Danish National Research Foundation (Centre for Materials Crystallography), and the Danish Research Council for Nature and Universe (Danscatt).

Supporting Information Available: Structure and chemical composition analysis of the intermediate products of the hierarchical structure corresponding to the morphologies of the SEM images in Figure 7a,b. This material is available free of charge *via* the Internet at http://pubs.acs.org.

REFERENCES AND NOTES

1. Harman, T. C.; Taylor, P. J.; Walsh, M. P.; LaForge, B. E. Quantum Dot Superlattice Thermoelectric Materials and Devices. *Science* **2002**, *297*, 2229–2232.
2. Heremans, J. P.; Jovovic, V.; Toberer, E. S.; Saramat, A.; Kurosaki, K.; Charoenphakdee, A.; Yamanaka, S.; Snyder, G. J. Enhancement of Thermoelectric Efficiency in PbTe by Distortion of the Electronic Density of States. *Science* **2008**, *321*, 554–557.
3. Chung, D.-Y.; Hogan, T.; Brazis, P.; Rocci-Lane, M.; Kannewurf, C.; Bastea, M.; Uher, C.; Kanatzidis, M. G. $CsBi_4Te_6$: A High-Performance Thermoelectric Material for Low-Temperature Applications. *Science* **2000**, *287*, 1024–1027.
4. Venkatasubramanian, R.; Siivola, E.; Colpitts, T.; O'Quinn, B. Thin-Film Thermoelectric Devices with High Room-Temperature Figures of Merit. *Nature* **2001**, *413*, 597–602.
5. Poudel, B.; Hao, Q.; Ma, Y.; Lan, Y.; Minnich, A.; Yu, B.; Yan, X.; Wang, D.; Muto, A.; Vashaee, D.; *et al.* High-Thermoelectric Performance of Nanostructured Bismuth Antimony Telluride Bulk Alloys. *Science* **2008**, *320*, 634–638.
6. Zhao, X. B.; Ji, X. H.; Zhang, Y. H.; Zhu, T. J.; Tu, J. P.; Zhang, X. B. Bismuth Telluride Nanotubes and the Effects on the Thermoelectric Properties of Nanotube-Containing Nanocomposites. *Appl. Phys. Lett.* **2005**, *86*, 062111-1–062111-3.
7. Hsu, K. F.; Loo, S.; Guo, F.; Chen, W.; Dyck, J. S.; Uher, C.; Hogan, T.; Polychroniadis, E. K.; Kanatzidis, M. G. Cubic $AgPb_mSbTe_{2+m}$: Bulk Thermoelectric Materials with High Figure of Merit. *Science* **2004**, *303*, 818–821.
8. Ma, Y.; Hao, Q.; Poudel, B.; Lan, Y.; Yu, B.; Wang, D.; Chen, G.; Ren, Z. Enhanced Thermoelectric Figure-of-Merit in p-Type Nanostructured Bismuth Antimony Tellurium Alloys Made from Elemental Chunks. *Nano Lett.* **2008**, *8*, 2580–2584.
9. Dresselhaus, M. S.; Chen, G.; Tang, M. Y.; Yang, R.; Lee, H.; Wang, D.; Ren, Z.; Fleurial, J.-P.; Gogna, P. New Directions for Low-Dimensional Thermoelectric Materials. *Adv. Mater.* **2007**, *19*, 1043–1053.
10. Mi, J. L.; Zhao, X. B.; Zhu, T. J.; Tu, J. P. Improved Thermoelectric Figure of Merit in n-Type $CoSb_3$ Based Nanocomposites. *Appl. Phys. Lett.* **2007**, *91*, 172116-1–172116-3.
11. Boukai, A. I.; Bunimovich, Y.; Tahir-Kheli, J.; Yu, J.-K; Goddard, W. A., III; Heath, J. R. Silicon Nanowires as Efficient Thermoelectric Materials. *Nature* **2008**, *451*, 168–171.
12. Hochbaum, A. I.; Chen, R.; Delgado, R. D.; Liang, W.; Garnett, E. C.; Najarian, M.; Majumdar, A.; Yang, P. Ehanced Thermoelectric Performance of Rough Silicon Nanowires. *Nature* **2008**, *451*, 163–167.

13. Harman, T. C.; Walsh, M. P.; Laforge, B. E.; Turner, G. W. Nanostructured Thermoelectric Materials. *J. Electron. Mater.* **2005**, *34*, L19–L22.
14. Toprak, M.; Zhang, Y.; Muhammed, M. Chemical Alloying and Characterization of Nanocrystalline Bismuth Telluride. *Mater. Lett.* **2003**, *57*, 3976–3982.
15. Foos, E. E.; Stroud, R. M.; Berry, A. D. Synthesis and Characterization of Nanocrystalline Bismuth Telluride. *Nano Lett.* **2001**, *1*, 693–695.
16. Fan, X. A.; Yang, J. Y.; Xie, Z.; Li, K.; Zhu, W.; Duan, X. K.; Xiao, C. J.; Zhang, Q. Q. Bi_2Te_3 Hexagonal Nanoplates and Thermoelectric Properties of n-Type Bi_2Te_3 Nanocomposites. *J. Phys. D: Appl. Phys.* **2007**, *40*, 5975–5979.
17. Sander, M. S.; Prieto, A. L.; Gronsky, R.; Sands, T.; Stacy, A. M. Fabrication of High-Density, High Aspect Ratio, Large-Area Bismuth Telluride Nanowire Arrays by Electrodeposition into Porous Anodic Alumina Templates. *Adv. Mater.* **2002**, *14*, 665–667.
18. Sander, M. S.; Gronsky, R.; Sands, T.; Stacy, A. M. Structure of Bismuth Telluride Nanowire Arrays Fabricated by Electrodeposition into Porous Anodic Alumina Templates. *Chem. Mater.* **2003**, *15*, 335–339.
19. Zhao, X. B.; Sun, T.; Zhu, T. J.; Tu, J. P. *In-Situ* Investigation and Effect of Additives on Low Temperature Aqueous Chemical Synthesis of Bi_2Te_3 Nanocapsules. *J. Mater. Chem.* **2005**, *15*, 1621–1625.
20. Zhang, G.; Yu, Q.; Yao, Z.; Li, X. Large Scale Highly Crystalline Bi_2Te_3 Nanotubes through Solution Phase Nanoscale Kirkendall Effect Fabrication. *Chem. Commun.* **2009**, 2317–2319.
21. Lu, W.; Ding, Y.; Chen, Y.; Wang, Z. L.; Fang, J. Bismuth Telluride Hexagonal Nanoplatelets and Their Two-Step Epitaxial Growth. *J. Am. Chem. Soc.* **2005**, *127*, 10112–10116.
22. Purkayastha, A.; Lupo, F.; Kim, S.; Borca-Tasciuc, T.; Ramanath, G. Low-Temperature, Template-Free Synthesis of Single-Crystal Bismuth Telluride Nanorods. *Adv. Mater.* **2006**, *18*, 496–500.
23. Zhang, G.; Wang, W.; Lu, X.; Li, X. Solvothermal Synthesis of V−VI Binary and Ternary Hexagonal Platelets: The Oriented Attachment Mechanism. *Gryst. Growth Des.* **2009**, *9*, 145–150.
24. Shi, W.; Zhou, L.; Song, S.; Yang, J.; Zhang, H. Hydrothermal Synthesis and Thermoelectric Transport Properties of Impurity-Free Antimony Telluride Hexagonal Nanoplates. *Adv. Mater.* **2008**, *20*, 1892–1897.
25. Yu, H.; Gibbons, P. C.; Buhro, W. E. Bismuth, Tellurium, and Bismuth Telluride Nanowires. *J. Mater. Chem.* **2004**, *14*, 595–602.
26. Cao, Y. Q.; Zhu, T. J.; Zhao, X. B.; Zhang, X. B.; Tu, J. P. Nanostructuring and Improved Performance of Ternary Bi−Sb−Te Thermoelectric Materials. *Appl. Phys. A: Mater. Sci. Process.* **2008**, *92*, 321–324.
27. Zhang, H. T.; Luo, X. G.; Wang, C. H.; Xiong, Y. M.; Li, S. Y.; Chen, X. H. Characterization of Nanocrystalline Bismuth Telluride (Bi_2Te_3) Synthesized by a Hydrothermal Method. *J. Cryst. Growth* **2004**, *265*, 558–562.
28. Deng, Y.; Nan, C.-W.; Wei, G.-D.; Guo, L.; Lin, Y.-H. Organic-Assisted Growth of Bismuth Telluride Nanocrystals. *Chem. Phys. Lett.* **2003**, *374*, 410–415.
29. DeSimone, J. M. Practical Approaches to Green Solvents. *Science* **2002**, *297*, 799–803.
30. Raveendran, P.; Fu, J.; Wallen, S. L. Completely "Green" Synthesis and Stabilization of Metal Nanoparticles. *J. Am. Chem. Soc.* **2003**, *125*, 13940–13941.
31. Lu, Q.; Gao, F.; Komarneni, S. Biomolecule-Assisted Reduction in the Synthesis of Single-Crystalline Tellurium Nanowires. *Adv. Mater.* **2004**, *16*, 1629–1632.
32. Feutelais, Y.; Legendre, B.; Rodier, N.; Agafonov, V. Study of the Phases in the Bismuth−Tellurium System. *Mater. Res. Bull.* **1993**, *28*, 591–596.
33. Peng, Q.; Dong, Y.; Li, Y. Synthesis of Uniform CoTe and NiTe Semiconductor Nanocluster Wires through a Novel Coreduction Method. *Inorg. Chem.* **2003**, *42*, 2174–2175.
34. Platzek, D.; Karpinski, G.; Stiewe, C.; Ziolkowski, P; Drasar, C.; Müller, E. Potential-Seebeck-Microprobe (PSM): Measuring the Spatial Resolution of the Seebeck Coefficient and the Electric Potential. *Proceedings of the 24th International Conference on Thermoelectrics* (ICT2005); IEEE, Clemson, SC, June, 2005; pp 13−16.